Introduction

Schoenberg (1980) proposed the linear slip boundary condition to describe the displacement discontinuity at a non-welded interface in terms of interface compliances. Hudson and Liu (1999) gave a more physical interpretation of the non-welded interface, by representing it as a planar distribution of cracks or a layer of cracked material with its thickness being small compared to the seismic wavelength. Reflection and transmission coefficients at non-welded interfaces are frequency-dependent. Van der Neut *et al.* (2007) showed how properties of a fault, such as fault thickness, crack density, crack infill and the presence of micro-corrugations can be directly related to the imaginary parts of the reflection coefficients at normal incidence.

A pore pressure drop in either the fault plane or its neighborhood induces an increase of the effective stress field, causing crack closures in the fault plane. This phenomenon is well described as it is the major source of stress induced velocity anisotropy, allowing time-lapse monitoring of effective stress fields in fractured media. We model the stress induced changes of crack properties in a fault. We investigate the use of complex-valued P- and S-wave reflection data at normal incidence with respect to the fault plane for monitoring the changing stress conditions with time-lapse observations.

Linear slip theory

Consider a horizontal non-welded interface in 3-dimensional space. In linear slip theory (Schoenberg, 1980) we assume that traction $\vec{\tau}_3$ is continuous at the interface, whereas there is a discontinuity of particle velocity $[\vec{v}]$ relating to the traction through interface compliance matrix $\mathbf{Z}$:

$$[\vec{v}] = i\omega \, \mathbf{Z} \, \vec{\tau}_3; \tag{1}$$

i denoting the complex unit and ω the angular frequency. We assume that $\mathbf{Z}$ has the following diagonal structure:

$$\mathbf{Z} = \begin{pmatrix} Z_T & 0 & 0 \\ 0 & Z_T & 0 \\ 0 & 0 & Z_N \end{pmatrix}; \tag{2}$$

Z_T and Z_N being the tangential and normal compliance respectively.

Reflection intercepts

We refer to the PP reflection coefficient at normal incidence as PP reflection intercept A^{PP}. Van der Neut *et al.* (2007) show that the real part of A^{PP} is hardly slip dependent. The imaginary part can be related directly to the interface slip, as long as the interface compliance is small with respect to the compliance of the background medium; it can be approximated by slip induced reflection intercept A_Ψ^{PP}:

$$A_\Psi^{PP} = -\left(\frac{1}{\rho_I \, \alpha_I} + \frac{1}{\rho_{II} \, \alpha_{II}} \right)^{-1} (1 - A_W^{PP}) \, \omega Z_N; \tag{3}$$

α and ρ being P-wave velocity and density, respectively; subscripts I and II relating to upper medium I and lower medium II; A_W^{PP} is the reflection intercept at an equivalent welded interface. As the reflection intercepts are complex-valued, both magnitude and phase of a reflecting wavelet will be modified. The slip induced reflection intercept can be related to these quantities as: $A_\Psi^{PP} \approx \Im(A^{PP}) = |A^{PP}| \sin \phi$; with $|A^{PP}|$ being the PP reflection magnitude at normal incidence and ϕ being the phase shift. Similar expressions can be derived for reflecting S-waves. We find for the slip induced SS reflection intercept (approximating the imaginary part of A^{SS}), with β being the S-wave velocity:

$$A_\Psi^{SS} = -\left(\frac{1}{\rho_I \, \beta_I} + \frac{1}{\rho_{II} \, \beta_{II}} \right)^{-1} (1 - A_W^{SS}) \, \omega Z_T. \tag{4}$$

Fault model

A fault can be interpreted as a layer with crack density e and fault thickness h, being small compared to the seismic wavelength. The cracks are evaluated in an average background medium with P-wave velocity $\bar{\alpha} = (\alpha_I + \alpha_{II})/2$, S-wave velocity $\bar{\beta} = (\beta_I + \beta_{II})/2$ and density $\bar{\rho} = (\rho_I + \rho_{II})/2$. We assume the cracks to be aligned with the fault plane, with the aspect ratios f having an exponential distribution with mean $\bar{f}$. We define the crack density ζ as:

$$\zeta = e\,h\,\left(1 + \frac{4\pi}{3}\left(\frac{h}{a}\,e\right)^{\frac{3}{2}}\right). \tag{5}$$

We can write for the tangential compliance (Hudson and Liu, 1999):

$$Z_T = \frac{16\bar{\alpha}^2}{3\bar{\rho}\,\bar{\beta}^2\,\left(3\bar{\alpha}^2 - 2\bar{\beta}^2\right)}\,\zeta. \tag{6}$$

It is well established that the tangential compliance is independent of crack infill, whereas the normal compliance is not. For 100% fluid saturation $Z_N^{FLUID} = 0$, whereas for 100% gas saturation (Hudson and Liu, 1999):

$$Z_N^{GAS} = \frac{4\bar{\alpha}^2}{3\bar{\rho}\,\bar{\beta}^2\,\left(\bar{\alpha}^2 - \bar{\beta}^2\right)}\,\zeta. \tag{7}$$

We define fluid indicator κ as $\kappa = Z_N/Z_T$, ranging from $\kappa = 0$ for fluid saturation to $\kappa = Z_N^{GAS}/Z_T$ for gas saturation. For a detailed review of the fluid indicator, see Shaw and Sen (2006).

Pore pressure changes

The effective stress σ_e is formally defined as:

$$\sigma_e = \sigma_f - n\,p; \tag{8}$$

p being the pore pressure, n being the dimensionless effective stress coefficient and σ_f the confining stress. As the pore pressure at a particular location drops with $-\Delta p$, effective stress will increase with $\Delta\sigma_e = n\,\Delta p$. For pore pressure drops outside the fault plane (as in a nearby hydrocarbon or water reservoir), changes in the effective stress field at the fault location can be computed through geomechanical modeling. The increase of effective stress results in crack squeezing; thus changing the aspect ratios f in the fault zone. Tod (2002) derived a linear relationship for this phenomenon, as described for a single crack (with $f \geq 0$):

$$f = f_0 - \frac{\bar{\alpha}^2}{\pi\,\bar{\rho}\,\bar{\beta}^2\,\left(\bar{\alpha}^2 - \bar{\beta}^2\right)}\,\Delta\sigma_e; \tag{9}$$

f_0 being the initial aspect ratio. Each crack has its critical stress level where $f = 0$; indicating crack closure. Since we assume an exponential distribution of aspect ratios in the fault, we can derive that the crack intensity decreases exponentially due to the crack closures as (Tod, 2002):

$$\zeta = \zeta_0\,\exp\left(-\frac{\bar{\alpha}^2}{\pi\,\bar{\rho}\,\bar{\beta}^2\,\left(\bar{\alpha}^2 - \bar{\beta}^2\right)\,\bar{f}}\,\Delta\sigma_e\right); \tag{10}$$

ζ_0 being the initial crack intensity. We use this expression to simulate the effect of a changing stress field on the crack intensity of the fault plane. This results in decreasing interface compliances through equations 6 and 7, thus affecting the imaginary parts of the reflection intercepts through equations 3 and 4. The complex valued reflection intercepts can thus be used to monitor the changing effective stress field in time-lapse observations.

	α	β	ρ
shale	2743	1394	2060
sand	2835	1762	2040

Table 1: Medium parameters (Castagna, 1993).
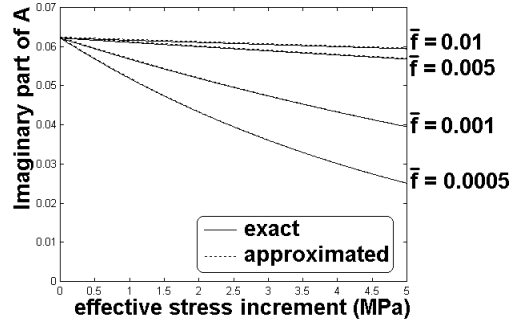
Figure 1: Imaginary part of the PP reflection intercept with increasing effective stress for various mean aspect ratios.

Example A: A fault in a static background medium

We consider a fault, represented as a thin layer of cracked material, with isotropic shale at its upper side and isotropic sandstone at its lower side; medium parameters are given in Table 1. Note that the interface contrast is very small, resulting in a small real part of the reflection intercept: $\Re(A^{PP}) \approx 0.01$. We assume the initial crack intensity to be $\zeta_0 = 0.3$. We compute the imaginary part of the P-wave reflection using an exact algorithm as well as equation 3 for various mean aspect ratios with varying effective stress increment $\Delta\sigma_e$ (Figure 1). The average aspect ratio turns out very crucial in this analysis. For $\bar{f} > 0.005$ we register hardly any stress dependence. We can thus conclude that faults with large and thin cracks have the most potential for stress monitoring.

Example B: A fault in a stress-dependent background

In realistic situations the background media will be stress dependent too. In the following example a fault cuts between two sandstones with a weak contrast. Properties of upper and lower media, being tight sands G13 and G14, are picked from Wang (2002) for both brine and gas saturated pore infill at a large stress interval; stress states $\sigma_e = 20.69MPa$, $\sigma_e = 34.48MPa$, $\sigma_e = 44.82MPa$ and $\sigma_e = 55.17MPa$ are considered. The tight sands are transverse isotropic, where we assume the axis of symmetry to be aligned with the normal of the fault plane. The fault is modeled as a thin layer of cracked material, where the crack intensity is initialized as $\zeta_0 = 0.3$ at $\sigma_e = 20.69MPa$. We assume the infill of cracks and surrounding pore space to be similar and the mean aspect ratio to be small: $\bar{f} = 0.001$. Fluid indicators are computed following Shaw and Sen (2006). The imaginary parts of the reflection intercepts are shown in Figure 2 and the real parts in Figure 3. Note that the effects of the changing stress field are well visible in the imaginary parts of both P- and S-wave data if the cracks are gas saturated. The brine saturated cracks can be monitored with S-waves only, as the fluid indicator (and thus the normal comliance) is too low in this situation (of the order $\kappa^{BRINE} \approx 0.01$). The real parts show no particular relationship with stress, other than the fluctuations caused by the changing contrast.
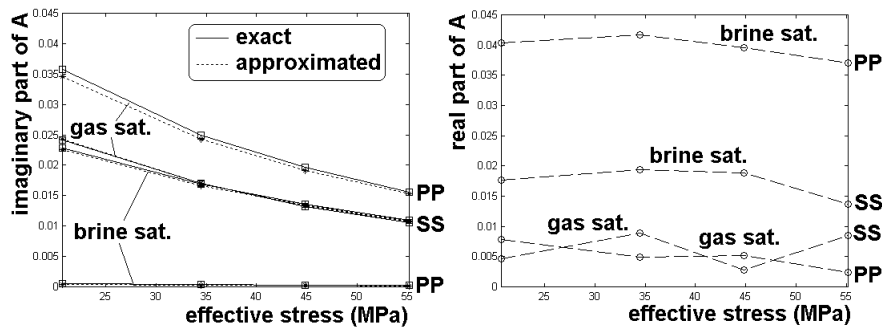
Figure 2: (left panel) Imaginary part of the reflection intercept for a large stress interval with a stress dependent background medium.

Figure 3: (right panel) Real part of the reflection intercept for a large stress interval with a stress dependent background medium.

Conclusion

We represented a fault as a thin layer of cracked material and derived how changing stress conditions affect the fault's properties as a seismic reflector. We showed how complex-valued P- and S-wave reflection coefficients at normal incidence with respect to the fault plane can monitor stress changes in time-lapse observations. The sensitivity of the reflection coefficients depends strongly on the aspect ratios of the cracks; faults with large and thin cracks have the most potential for stress monitoring. Complex-valued P-wave reflection data is highly dependent on the crack infill and most useful for stress monitoring of gas saturated fault planes. Complex-valued S-wave reflection data is independent on the crack infill and can be used for stress monitoring of both gas and fluid saturated faults.

References

Castagna, J. P. [1993] *Amplitude-versus-offset-dependent reflectivity - theory and practice of avo analysis* Tulsa, OK: Society of Exploration Geophysicists.

Hudson, J. A., and Liu, E. [1999] Effective elastic properties of heavily faulted structures. *Geophysics* 64, 479–485.

Schoenberg, M. [1980] Elastic wave behavior across linear slip interfaces. *Journal of the Acoustical Society of America* 68, 1516–1521.

Shaw, R. K., and Sen, M. K. [2006] Use of avoa data to estimate fluid indicator in a vertically fractured medium. *Geophysics* 71, C15–C24.

Tod, S. R. [2002] The effects of stress and fluid pressure on the anisotropy of interconnected cracks. *Geophysical Journal International* 149, 149–156.

Van der Neut, J. R., Sen, M. K. and Wapenaar, K. [2007] *Seismic reflections at faults: a model study* 69th Conference and Exhibition, EAGE.

Wang, Z. [2002] Seismic anisotropy in sedimentary rocks, part 2: Laboratory data. *Geophysics* 67, 1423–1440.